

## Droplet breakup in flow past an obstacle: A capillary instability due to permeability variations

This article has been downloaded from IOPscience. Please scroll down to see the full text article.

2010 EPL 92 54002

(<http://iopscience.iop.org/0295-5075/92/5/54002>)

View [the table of contents for this issue](#), or go to the [journal homepage](#) for more

Download details:

IP Address: 18.111.10.153

The article was downloaded on 04/01/2011 at 19:13

Please note that [terms and conditions apply](#).

# Droplet breakup in flow past an obstacle: A capillary instability due to permeability variations

S. PROTIÈRE<sup>1(a)</sup>, M. Z. BAZANT<sup>2</sup>, D. A. WEITZ<sup>1</sup> and H. A. STONE<sup>3</sup>

<sup>1</sup> *Department of Physics and SEAS, Harvard University - Cambridge, MA 02138, USA*

<sup>2</sup> *Departments of Chemical Engineering and Mathematics, MIT - Cambridge, MA 02139, USA*

<sup>3</sup> *Department of Mechanical and Aerospace Engineering, Princeton University - Princeton, NJ 08544, USA*

received 27 September 2010; accepted in final form 16 November 2010

published online 22 December 2010

PACS 47.55.df – Breakup and coalescence

PACS 47.50.Gj – Instabilities

PACS 47.56.+r – Flows through porous media

**Abstract** – In multiphase flow in confined geometries an elementary event concerns the interaction of a droplet with an obstacle. As a model of this configuration we study the collision of a droplet with a circular post that spans a significant fraction of the cross-section of a microfluidic channel. We demonstrate that there exist conditions for which a drop moves completely around the obstacle without breaking, while for the same geometry but higher speeds the drop breaks. Therefore, we identify a critical value of the capillary number above which a drop will break. We explain the results with a one-dimensional model characterizing the flow in the narrow gaps on either side of the obstacle, which identifies a surface-tension-driven instability associated with a variation in the permeability in the flow direction. The model captures the major features of the experimental observations.

Copyright © EPLA, 2010

**Introduction.** – Microfluidic technologies as a platform for manipulating droplets are providing new approaches for designer emulsions [1], encapsulation of molecules and cells [2], high-throughput biological assays [3], kinetic analyses [4], and detection of surface contamination [5]. Continued developments of such multiphase flows requires understanding and control of droplet traffic [6], drop breakup [7], and drop coalescence [8]. For example, new insights into the latter topic have come from microfluidic studies of controlled coalescence using extensional flows [9] and electric fields [10].

The motion of drops in confined geometries is also relevant to traditional subjects such as multiphase flow in porous media, the motion of drops in networks of channels [11], and for understanding physiological flows, which are relevant to airway re-opening [12,13]. One direction for improved understanding of these flows is to quantify breakup in confined flows, *e.g.*, past studies have reported and rationalized drop breakup at T-junctions [14–16] or in a constricted cylindrical capillary [17].

In this study we investigate the breakup of drops flowing past an obstacle. Previous work showed it was possible to break drops in such flows, but no quantitative measurements were provided [14]. Some features of the influence of various obstruction shapes, including experiments and numerics, have been reported recently [18]. Here we describe the case where a drop that is significantly larger than the gap or channel can squeeze past the occlusion without breaking; we focus on understanding the conditions for breakup. We identify a critical capillary number below which drops do not break and above which drops break. Finally, we explain this transition in terms of an instability of the menisci located in the narrow gaps on either side of the obstacle and provide a one-dimensional theory that rationalizes the results qualitatively.

**Experimental setup.** – We disperse droplets of hexadecane (viscosity  $\eta_{drop} = 8 \times 10^{-3}$  Pa s) in a continuous phase of distilled water (viscosity  $\eta_{cont} = 1 \times 10^{-3}$  Pa s). A surfactant, sodium dodecyl sulfate (SDS) at 1 wt.% is added to the water to stabilize the droplets against coalescence. The interfacial tension between the surfactant solution and hexadecane is  $\gamma \approx 5 \times 10^{-3}$  N/m, as measured using a ring tensiometer.

<sup>(a)</sup>Present address: Institut Jean le Rond d'Alembert, CNRS/UPMC UMR 7190 - 75252 Paris Cedex 05, France, EU; E-mail: protiere@ida.upmc.fr

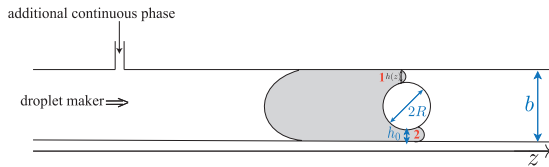


Fig. 1: (Colour on-line) Schematic of the experiment. A drop of viscosity  $\eta_{drop}$  is dispersed in a continuous phase (viscosity  $\eta_{cont}$ ) flowing from left to right and meeting a circular obstruction.

Syringe pumps are used to control the flow rates of the fluids in the microfluidic devices, which are fabricated in poly(dimethylsiloxane) (PDMS) using soft lithography techniques [19]. The channels are  $w = 50 \mu\text{m}$  high and  $b = 120 \mu\text{m}$  wide (fig. 1) and remain hydrophilic for the duration of an experiment as the water-SDS solution is infused after the devices undergo oxygen plasma treatment. We have also studied the inverse experiment where the outer phase is hexadecane and the dispersed liquid is the water-SDS solution. In this case we do not need to infuse the outer fluid immediately after oxygen plasma treatment.

Droplets are generated upstream at a T-junction [14] or using a flow-focusing method [20] far upstream of the post so the flow can be considered steady near the obstacle. The drops are larger than the channel width and are therefore “pancake” shaped, with the size set by the continuous-phase flow rate. Injection of additional outer phase fluid downstream of the droplet maker allows the continuous-phase flow rate to be varied independently of the drop size.

An obstruction in the form of a circular post in the center of the channel is placed downstream of where the drops are first formed (fig. 1). We vary the obstacle’s radius  $R$  so as to control the minimum distance to the sidewall  $h_0$ . We estimate the droplet volume through image analysis by measuring its length and considering it as a rectangle connected by two hemi-disks of width  $w$ . The motion of the drop near the obstacle is recorded using a fast camera (Phantom V7).

The non-dimensional drop speed, represented as a capillary number,  $\mathcal{C} = \eta_{drop}Q/bw\gamma$ , compares the magnitude of viscous forces to the surface tension force, where  $Q$  is the total flow rate of the continuous phase. Capillary numbers in our experiments span between  $0.01 < \mathcal{C} < 0.12$ . Depending on the speed of the drop, we observe two very different responses when a drop encounters an obstacle.

**A critical capillary number for breakup.** – The first drop response, observed at higher capillary numbers, corresponds to the drop breakup into two daughter drops of different sizes following collision with the obstacle (fig. 2(a)–(e)); in the experiments the drop has a viscosity 8 times that of the continuous phase. When the drop first meets the obstacle, the liquid-liquid menisci fill the two gaps on either side of the obstruction though the dynamics on the two sides are not identical, and the drop breaks. Generally, the two drops formed are of different sizes.

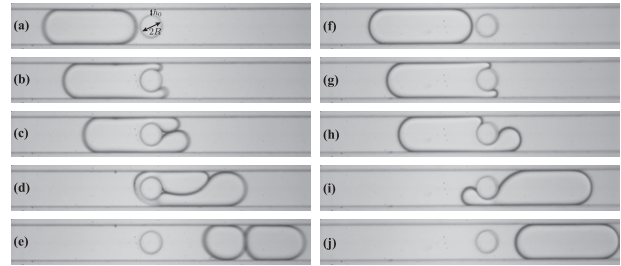


Fig. 2: Sequence of images showing a drop approaching an obstacle (circular post of radius  $R = 40 \mu\text{m}$ ,  $h_0 = 20 \mu\text{m}$ ) for two values of  $\mathcal{C}$ ;  $\eta_{drop}/\eta_{cont} = 8$ . Images (a)–(e)  $\mathcal{C} = 0.06$ . (a)  $t = 0$  ms. The drop collides with the post. (b)  $t = 2.5$  ms. The meniscus in the lower gap is slightly ahead of the meniscus in the upper gap. (c)  $t = 5$  ms. The drop is distorted and is splitting as it flows through both gaps past the obstacle. (d)  $t = 11.5$  ms. The drop is almost split into two. (e)  $t = 17.5$  ms. Downstream of the post the drop has split into two drops of different sizes. Images (f)–(j):  $\mathcal{C} = 0.012$ . (f)  $t = 0$  ms. The drop meets the post. (g)  $t = 20$  ms. The meniscus in the lower gap is ahead of the meniscus in the upper gap. (h)  $t = 30$  ms. The meniscus in the upper gap is moving backwards. (i)  $t = 70$  ms. The entire drop passes through the lower gap. (j)  $t = 82.5$  ms. The drop has passed the obstacle without breaking up.

A different response is observed at lower capillary numbers (see fig. 2(f)–(j)). In this case, the drop menisci enter the gaps on both sides of the obstacle: when the meniscus in the upper gap is about half-way past the post, it gradually retracts (see fig. 2(h) and (i)), while the liquid in the lower gap moves continually forward until finally the entire drop has passed the obstacle only through the lower gap. Thus, we have illustrated a critical capillary number for breakup: at low  $\mathcal{C}$ , drops do not break in spite of significant deformation caused by the collision with the obstacle, while for higher  $\mathcal{C}$  drops break.

To understand these two different responses, we follow the drop’s axial position ( $z$ ) along the channel on both sides of the gap as a function of time. At higher capillary numbers, the two leading menisci move at nearly the same speed upon first colliding with the obstruction (fig. 3, curves A and B). However, when the menisci have reached half-way around the post, one meniscus moves a little faster in one gap compared to the other. These dynamics lead to the formation of two drops of different sizes. When the drop meets the post at a smaller capillary number, the menisci enter each gap (fig. 3, curves C and D) and we observe that the liquid is slightly ahead in one gap compared to the other gap. Nevertheless, when the menisci have traveled about half-way around the post, we observe that the leading meniscus suddenly moves faster whereas the meniscus in the other gap reverses its motion and the drop does not break. This dynamical response occurs even though the average axial pressure drop is directed downstream.

To further investigate this breakup phenomenon we have measured the size of the droplets formed after breakup when the initial speed of the drop is increased

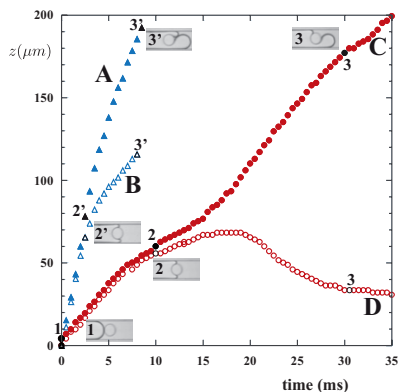


Fig. 3: (Colour on-line) Position of the menisci as a function of time in the lower (A and C) and upper (B and D) gaps;  $\eta_{drop}/\eta_{cont} = 8$ .  $C = 0.06$  for curves A and B, where the drop breaks.  $C = 0.012$  for curves C and D, where the drop does not break. Each numbered image shows the position of the drop with the menisci evident.

gradually (fig. 4). The results are reported as  $V_{out}/V_{in}$ , where  $V_{in}$  is the initial volume of the drop and  $V_{out}$  is the volume of the daughter drops formed after the collision with the post. At capillary numbers below a critical value  $C_{cr}$ , the drop passes the obstruction through one gap without breaking. We have found that the critical conditions for the breaking/non-breaking transition appear to depend only weakly on the aspect ratio of the gap  $h_0/b$  (fig. 4(a)). For increasing values of  $C > C_{cr}$  the two daughter drops become more comparable in size (fig. 4).

We have also performed a few experiments to determine that the critical value of the capillary number  $C_{cr}$  depends strongly on the viscosity ratio of the liquids. Figure 4(b) shows that a drop with  $\eta_{drop}/\eta_{cont} = 8$  breaks for  $C_{cr} \approx 0.02$  while for a  $\eta_{drop}/\eta_{cont} = 1/8$  the drop breaks at the smallest flow rates we were able to access,  $C_{cr} \rightarrow 0$ .

**One-dimensional model of the instability.** – We now develop an analytical description to describe the experimental observations of the two typical behaviors described above for the collision of a drop with a post in the confined space of a channel. We observed that either the drop i) splits, which corresponds to the invasion of the channels on either side of the post, or ii) goes around the post without splitting. We interpret these two different responses as a hydrodynamic instability, where the two menisci initially move together around the post but are “unstable” for case ii) so that only one meniscus ends up bypassing the post, while the “stable” state of invasion of both sides of the post produces two drops (case i)). The description at this stage is qualitative since the breaking of the drop into two smaller drops also exhibits menisci that move at different speeds, though the speed difference is reduced as the capillary number is increased (figs. 3 and 4).

These dynamics have the spirit of the Saffman-Taylor instability, which refers to the finger-like propagation of low-viscosity fluid during displacement of a fluid of higher

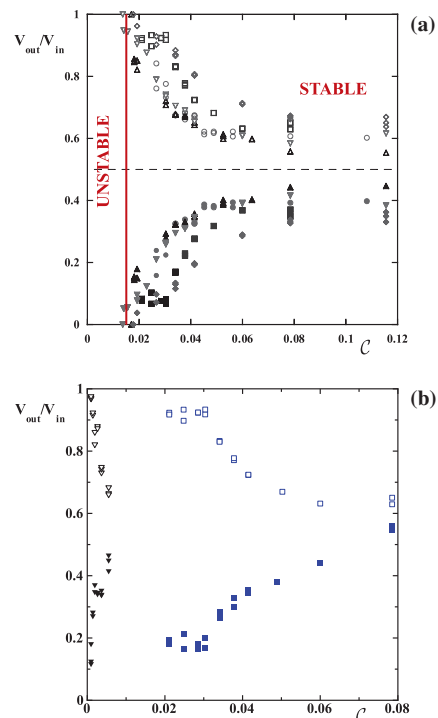


Fig. 4: (Colour on-line) (a) Volume of the daughter drops  $V_{out}$  normalized by the initial volume of the drop  $V_{in}$  as a function of the capillary number  $C$ . We measure the length or diameter of the drop,  $D$  to estimate its volume. When the drop is pancake-shaped we estimate it to be that of a rectangle connected by two hemi-disks of width  $w$ . The open symbols correspond to the volume of the first daughter drop to pass the obstacle and the full symbols to the volume of the second daughter drop. Circles:  $h_0/b = 1/12$ , squares:  $h_0/b = 1/6$ , triangles:  $h_0/b = 1/4$ , inverted triangles:  $h_0/b = 1/3$ , diamonds:  $h_0/b = 5/12$ . (b)  $V_{out}/V_{in}$  as a function of  $C$  with  $h_0/b = 1/6$  for two different viscosity ratios; squares  $\eta_{drop}/\eta_{cont} = 8$  and triangles  $\eta_{drop}/\eta_{cont} = 1/8$ .

viscosity [21,22]. Nevertheless, our measurements, which occur at a constant flow rate, demonstrate an instability of a propagating meniscus even when the drop phase is more viscous than the continuous phase (fig. 2), which is the “stable” state in a classical viscous fingering configuration. Moreover, the instability we observe is most significant for the largest values of the surface tension, *i.e.* lower capillary numbers, which also is in contrast with the usual descriptions of viscous fingering. As we describe below with a one-dimensional model, the control parameter for the instability when multiple connected menisci travel along parallel paths is the permeability ( $k$ ) variation in the flow direction in the gaps on either side of the obstacle. The one-dimensional analysis has similarities with the study of bubble propagation in branching microfluidic networks [12], though the qualitative trends we identify are distinct.

Consider a fluid of viscosity  $\lambda\eta$  invading a channel of variable shape filled with wetting fluid of viscosity  $\eta$ ; for the experiments shown in fig. 2 we identify  $\eta = \eta_{cont}$  and

$\lambda = \eta_{drop}/\eta_{cont}$ . The positions of the menisci ( $i = 1, 2$ ) in either gap are denoted  $z_i(t)$ . The one-dimensional flow in either phase is described by the Darcy equation, relating the velocities and pressures of the two fluids,

$$z < z_i(t): \frac{\lambda \eta u}{k} = -\frac{\partial p}{\partial z}, \quad z > z_i(t): \frac{\eta \hat{u}}{k} = -\frac{\partial \hat{p}}{\partial z}. \quad (1)$$

We assume that the invading fluid completely fills the channel and neglect the influence of wetting films (*e.g.* [12]). The permeability of the ‘‘channels’’ (*i.e.* the gaps on either side of the post) varies with  $z$  and, within the familiar lubrication approximation where the channel height  $h(z)$  is much smaller than the width  $b$  or the obstacle radius  $R$ , we have  $k(z) = \frac{h(z)^2}{12} = \frac{h^2}{\beta^2}$ . For the configuration of flow around the post, we approximate the variation of the gap as  $h(z) = h_0 \left(1 + \frac{z^2}{2h_0 R}\right)$ , which identifies the characteristic length  $\ell = (2h_0 R)^{1/2}$  in the flow direction along the gap. Similarly, there is a pressure drop across the curved liquid-liquid interface, which we write approximately as  $p - \hat{p} = \frac{c\gamma}{k^{1/2}(z_i)}$ , where the constant  $c = O(1)$  and the dominant radius of curvature is assumed proportional to the local channel height (or  $k^{1/2}$ ). The (two-dimensional) flow rate  $q_i$  through either side of the post can vary in time, and the value is set following the motion of the meniscus at position  $z_i(t)$ :

$$q_i(t) = h(z)u(z, t) = \beta k^{1/2}(z_i) \frac{dz_i}{dt}. \quad (2)$$

Thus, assuming that the pressure variations are localized to the gap between the post and channel boundaries, which is a good approximation in lubrication configurations, we integrate the Darcy equations (1) from upstream of the post (pressure  $p_0(t)$ ) to downstream (pressure  $p_\infty(t)$ ), which leads to ( $i = 1, 2$ )

$$\eta k^{1/2}(z_i) \frac{dz_i}{dt} \left( \lambda \int_0^{z_i(t)} \frac{dz}{k^{3/2}} + \int_{z_i(t)}^\infty \frac{dz}{k^{3/2}} \right) = p_0 - p_\infty - \frac{c\gamma}{k^{1/2}(z_i)}. \quad (3)$$

Writing this equation for the two menisci individually,  $i = 1$  and  $i = 2$ , and then subtracting eliminates the pressure difference, and yields

$$k^{1/2}(z_1) \frac{dz_1}{dt} \left( \lambda \int_0^{z_1(t)} \frac{dz}{k^{3/2}} + \int_{z_1(t)}^\infty \frac{dz}{k^{3/2}} \right) - k^{1/2}(z_2) \frac{dz_2}{dt} \left( \lambda \int_0^{z_2} \frac{dz}{k^{3/2}} + \int_{z_2}^\infty \frac{dz}{k^{3/2}} \right) = \frac{c\gamma}{\eta} \left( \frac{1}{k^{1/2}(z_2)} - \frac{1}{k^{1/2}(z_1)} \right). \quad (4)$$

Along with mass conservation, where the constant flow rate (per unit width)  $q_0$  satisfies  $q_0 = \beta k^{1/2}(z_1) \frac{dz_1}{dt} + \beta k^{1/2}(z_2) \frac{dz_2}{dt}$ , we now have two equations for two unknown menisci positions,  $z_1(t)$  and  $z_2(t)$ .

It is convenient to nondimensionalize the equations with

$$K = \frac{k}{h_0^2/\beta^2}, \quad Z = \frac{z}{\ell}, \quad \tau = \frac{t}{\ell h_0/q_0}, \quad (5)$$

in which case we arrive at the two equations

$$K^{1/2}(Z_1) \frac{dZ_1}{d\tau} \left( \lambda \int_0^{Z_1(\tau)} \frac{dZ}{K^{3/2}} + \int_{Z_1(\tau)}^\infty \frac{dZ}{K^{3/2}} \right) - K^{1/2}(Z_2) \frac{dZ_2}{d\tau} \left( \lambda \int_0^{Z_2(\tau)} \frac{dZ}{K^{3/2}} + \int_{Z_2(\tau)}^\infty \frac{dZ}{K^{3/2}} \right) = \frac{\lambda}{\mathcal{C}_{\text{eff}}} \left( \frac{1}{K^{1/2}(Z_2)} - \frac{1}{K^{1/2}(Z_1)} \right), \quad (6)$$

and

$$1 = K^{1/2}(Z_1) \frac{dZ_1}{d\tau} + K^{1/2}(Z_2) \frac{dZ_2}{d\tau}, \quad (7)$$

where  $\mathcal{C}_{\text{eff}} = \frac{\beta \eta_{drop} q_0 \ell}{c \gamma h_0^2}$  is defined using the drop viscosity to be consistent with the experiments. This system of equations gives the time-dependent positions of the menisci  $Z_1(\tau)$  and  $Z_2(\tau)$  as a function of two dimensionless parameters,  $\mathcal{C}_{\text{eff}}$  and  $\lambda$ . The response also depends on the spatial variation of the channel permeability  $K(Z)$ .

For the case of a narrow parabolic gap between the cylindrical post and the boundary we have  $K = (1 + Z^2)^2$ . Performing the integration in eq. (6) and rearranging using (7) leads to

$$2(1 + Z_1^2) \frac{dZ_1}{d\tau} = \frac{1 + \frac{2}{\pi}(\lambda - 1)\mathcal{L}(Z_2) + \frac{16\lambda}{3\pi\mathcal{C}_{\text{eff}}} \left( \frac{Z_1^2 - Z_2^2}{(1 + Z_1^2)(1 + Z_2^2)} \right)}{1 + \frac{2}{\pi}(\lambda - 1)(\mathcal{L}(Z_1) + \mathcal{L}(Z_2))}, \quad (8)$$

where  $\mathcal{L}(Z) = \arctan(Z) + \frac{Z}{1 + Z^2} + \frac{2}{3} \frac{Z}{(1 + Z^2)^2}$ .

We next analyze the linear stability of these equations. The base state corresponds to both menisci moving at the same speed with time-dependent position  $Z_0 + \frac{1}{3}Z_0^3 = \frac{1}{2}\tau$ , where we have chosen  $Z(0) = 0$ . Thus, we seek perturbations to this base state of the mass-conserving form

$$Z_1 = Z_0 + \delta(\tau) \quad \text{and} \quad Z_2 = Z_0 - \delta(\tau) \quad \text{with} \quad \delta \ll 1. \quad (9)$$

If we further assume that  $Z_0 \ll 1$ , then (9) leads to growth of the perturbation according to

$$\frac{1}{\delta} \frac{d\delta}{d\tau} = \frac{16}{3\pi} \left( \frac{4\lambda Z_0}{\mathcal{C}_{\text{eff}}} - (\lambda - 1) \right). \quad (10)$$

We compare the dimensional form of this estimate for the growth rate of the instability (treating  $Z_0(\tau)$  as an order-one quantity) with the typical time ( $\ell/(q_0/h_0)$ ) to bypass the obstacle. When this ratio is less than 1 we expect an instability where one meniscus grows at a much faster rate than the other meniscus can propagate to the other side of the obstacle. Hence, the unstable state, which

we have seen to produce no breakup of the drop, occurs when

$$\text{“instability”}: \frac{\lambda}{C_{\text{eff}}} - (\lambda - 1) > 1 \quad \text{or} \quad C_{\text{eff}} < 1. \quad (11)$$

The fact that this prediction is independent of  $\lambda$  suggests that to account for the viscosity ratio dependence requires a fully nonlinear calculation.

This one-dimensional calculation makes two predictions consistent with the experimental observations. First, we identify a critical capillary number above which the menisci positions are “stable” and two drops are formed, which is consistent with the qualitative trends reported in the experiments. Lower capillary numbers are predicted to be more unstable. Second, the above argument shows that when the meniscus is upstream of the post  $Z_0 < 0$ , the menisci movements are stable, which is consistent with our observations in that the instability only sets in when the menisci advance beyond the position of the minimum gap.

We can use the nonlinear theory to examine the dynamics as the capillary number is varied, in the spirit of the experimental results for the menisci positions shown in fig. 3. In order to capture the manner in which the experiment is performed, where the capillary number is changed by varying the flow rate, we plot the dimensionless results in terms of the dimensionless time scale  $\tau/C_{\text{eff}}$ . In particular, we advance the menisci into the widening gap according to the unperturbed solution  $Z_0(\tau)$  and at time  $\tau = 1/4$  introduce a small perturbation.

As an example, for  $\lambda = 8$  we numerically solve the two ordinary differential equations for  $Z_1(\tau)$  and  $Z_2(\tau)$  for  $C_{\text{eff}} = 0.06$  and  $C_{\text{eff}} = 0.8$ , which are, respectively, below and above the critical capillary number for instability (lower capillary numbers are more unstable). The numerical results are shown in fig. 5(a). We observe that for the smaller capillary number the positions of the two menisci diverge as the leading one advances into the diverging gap, and, more significantly, the trailing meniscus begins to retract. For the larger capillary number, the two menisci continue to advance at nearly the same rate, and the perturbation has only a minor effect. These dynamical features are consistent with the most significant trends evident in fig. 3. Similar calculations for lower  $\lambda$  show that the critical capillary number  $C_{\text{eff,cr}}$  for the instability is monotonically reduced, with more rapid variations for  $\lambda < 1$  (fig. 5(b)). The trend is consistent with the experimental results though the magnitude of the change is not as large.

The above ideas can be generalized to use the one-dimensional approach with arbitrary shape functions (but with consistency within the lubrication approximations) and with the droplet or interface advancing into a region of  $N$  identical subchannels. In this case it is convenient to give the steps in dimensional form. Again, we let  $k(z)$  denote the permeability, and introduce  $\kappa(z)$  as the mean curvature of the meniscus, and  $a(z)$  the cross-sectional area (the geometry need not be planar). The hydraulic

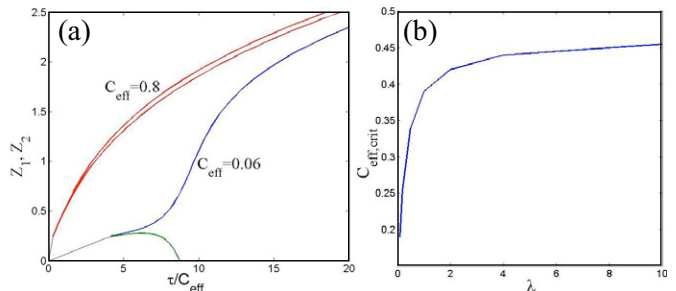


Fig. 5: (Colour on-line) (a) Numerical solutions for the menisci position as a function of the dimensionless time  $\tau/C_{\text{eff}}$  for  $C_{\text{eff}} = 0.8$  and  $C_{\text{eff}} = 0.06$ ;  $\lambda = 8$ . We observe the same behavior as the experimental results shown in fig. 3. (b) Numerically estimated critical capillary number for an instability,  $C_{\text{eff,cr}}$ , vs.  $\lambda$ .

resistance of a subchannel of length  $L$  with a meniscus at position  $z_i$  is given by

$$R(z_i; \lambda) = \lambda \int_0^{z_i} \frac{dz'}{k(z')a(z')} + \int_{z_i}^L \frac{dz'}{k(z')a(z')}. \quad (12)$$

Let  $\Delta p(t) > 0$  be the total pressure drop across the subchannels from the inlet to the reservoir downstream. The flow rate  $Q_i(t)$  in each subchannel satisfies a system of nonlinear first-order differential equations:

$$Q_i = a(z_i) \frac{dz_i}{dt} = \frac{\Delta p - \gamma \kappa(z_i)}{R(z_i)}. \quad (13)$$

The pressure  $\Delta p(t)$  is determined implicitly by the constraint of fixed total flow rate  $Q_0 = \sum_i Q_i$ , which provides a nonlinear coupling among the menisci.

Suppose the menisci move together, leading to symmetric breakup into  $N$  identical daughter droplets. Then, the average meniscus position  $z_i(t) = \bar{z}(t)$  is given by

$$Q_1 = \frac{Q_0}{N} = a(\bar{z}) \frac{d\bar{z}}{dt}, \quad (14)$$

with solution  $\bar{z}(t) = V^{-1}(Q_1 t)$ , where  $V(z)$  is the subchannel volume from 0 to  $z$ , which satisfies  $V'(z) = a(z)$ . In order to maintain the total flow rate, the pressure varies as  $\Delta \bar{p}(t) = Q_1 R(\bar{z}(t)) + \gamma \kappa(\bar{z}(t))$ .

We now consider a small perturbation of the base state,  $z_i(t) = \bar{z}(t) + \delta_i(t)$ , where  $|\delta_i| \ll \bar{z}$  and derive a linear system for  $\delta_i(t)$ . Since the mean perturbation (a linear combination) is preserved under linearized dynamics, we can set it to zero without loss of generality,  $\sum_i \delta_i = 0$ . With this choice,  $\bar{z}(t)$  is the mean position of the menisci for all times in the linear regime. Next, we linearize (13) to obtain the generalization of equation (10) in the form

$$\frac{1}{\delta_i} \frac{d\delta_i}{dt} = \alpha(\bar{z}(t)), \quad (15)$$

which has the general solution  $s_i(t) = s_i(0) \exp(\int_0^t \alpha(\bar{z}(\tau)) d\tau)$ , where the local exponential growth

rate of perturbations depends only the mean meniscus position, given by

$$\alpha(z) = -\frac{\gamma\kappa'(z)a(z) + Q_1(a(z)R(z))'}{a(z)^2R(z)} \quad (16)$$

Regions of linear instability in the subchannels are defined by the condition  $\alpha(\bar{z}) > 0$ . Outside these regions the synchronized base state is stable. Since the menisci enter the subchannels in a nearly synchronized state, we can predict the *critical position*,  $z_c = \min_z \{z : \alpha(z) > 0\}$ , where the linear instability begins for a given geometry (if  $z_c < L$ ).

For a given geometry, we can interpret the linear instability condition  $\alpha > 0$  as a bound on an effective local capillary number. Therefore, we conclude

$$\text{linear instability: } \frac{Q_0(a(z)R(z))'}{N\gamma|\kappa'(z)|a(z)} < 1, \quad (17)$$

which is a geometrical criterion for linear instability that generalizes the result above for an obstruction with two parabolic gaps. The viscosity ratio implicitly enters the analysis through the resistivity.

As an example, suppose that a more viscous fluid is invading a less viscous wetting fluid,  $\lambda > 1$ . In that case, the channel resistance increases with meniscus position,  $R \propto z$ . For consistency with the lubrication approximation, we must have  $(a(z)z)' > 0$ , so that the cross-sectional area varies slowly with subchannel length. Since hydraulic resistance increases with length, the last term in (16) must be positive in the lubrication limit. The meniscus curvature  $\kappa(z)$  scales with the inverse of the channel width. We conclude that for thin channels the menisci are *stable in contracting regions* ( $\kappa' > 0$ ) and can be *unstable in expanding regions* ( $\kappa' < 0$ ), consistent with both experiments and the simpler version of the theory.

**Discussion.** – This problem of displacement of one fluid by a second fluid is the origin of the classical viscous fingering instability [21,22]. In particular, it is well known that when a low-viscosity fluid invades a Hele-Shaw cell filled with high-viscosity fluid, a propagating finger of low-viscosity fluid develops, thus bypassing the mostly stationary higher-viscosity fluid. However, invading fluid more viscous than the emplaced fluid propagates with a uniform front. Here we show that when a viscous droplet, large compared to the channel width, meets an obstacle partially blocking a channel filled with lower-viscosity fluid, there is a critical speed above which the viscous liquid drop breaks into two different-sized drops and below which all of the fluid bypasses the obstacle through only one of the gaps. An instability in the relative motion of the two menisci will prevent a drop from breaking at very low capillary numbers, so that there exists a critical value of the capillary number  $C_{cr}$ . A theoretical description of this instability was given in the form of a one-dimensional model that recognizes permeability variations in the flow direction. The model captures the most significant qualitative trends present

in the experimental results. From a fundamental point of view, our study provides new results concerning the control of droplets in a microfluidic channel. In a more global context, our quantification of the breakup process can yield a better understanding of droplet flow in all types of porous media.

\*\*\*

The authors thank A. T. KRUMMEL, E. DRESSAIRE, M. HURLIMANN and D. L. JOHNSON for helpful discussions. We also thank Schlumberger-Doll Research and the Harvard MRSEC (DMR-0820484) for support.

## REFERENCES

- [1] UTADA A. S., CHU L. -Y., FERNANDEZ-NIEVES A., LINK D. R., HOLTZE C. and WEITZ D. A., *MRS Bull.*, **32** (2007) 702.
- [2] EDD J. F., DI CARLO D., HUMPHRY K. J., KOESTER S., IRIMIA D., WEITZ D. A. and TONER M., *Lab Chip*, **8** (2008) 1262.
- [3] THORSEN T., MAERKL S. J. and QUAKE S. R., *Science*, **298** (2002) 580.
- [4] SONG H., TICE J. D. and ISMAGILOV R., *Angew. Chem., Int. Ed.*, **42** (2003) 768.
- [5] BOEDICKER J. Q., LI L., KLINE T. R. and ISMAGILOV R. F., *Lab Chip*, **8** (2008) 1265.
- [6] ENGL W., ROCHE M., COLIN A., PANIZZA P. and AJDARI A., *Phys. Rev. Lett.*, **95** (2005) 208304.
- [7] BIBETTE J., *J. Colloid Interface Sci.*, **147** (1991) 474.
- [8] NIU X., GULATI S., EDEL J. B. and DEMELLO A. J., *Lab Chip*, **8** (2008) 1837.
- [9] BREMOND N., THIAM A. R. and BIBETTE J., *Phys. Rev. Lett.*, **100** (2008) 024501.
- [10] THIAM A. R., BREMOND N. and BIBETTE J., *Phys. Rev. Lett.*, **102** (2009) 188304.
- [11] STARK J. and MANGA M., *Transp. Porous Media*, **40** (2000) 201.
- [12] BAROUD C. N., TSIKATA S. and HEIL M., *J. Fluid Mech.*, **546** (2006) 285.
- [13] CALDERÓN A. J., FOWLKES J. B. and BULL J. L., *J. Appl. Physiol.*, **99** (2005) 479.
- [14] LINK D. R., ANNA S. L., WEITZ D. A. and STONE H. A., *Phys. Rev. Lett.*, **92** (2004) 054503.
- [15] MÉNÉTRIER-DEREMBLE L. and TABELING P., *Phys. Rev. E*, **74** (2006) 035303.
- [16] LESHANSKY A. M. and PISMEN L. M., *Phys. Fluids*, **21** (2009) 023303.
- [17] GAUGLITZ P. A., ST LAURENT C. M. and RADKE C. J., *Ind. Eng. Chem. Res.*, **27** (1988) 1282.
- [18] CHUNG C., LEE M., CHAR K., AHN K. H. and LEE S. J., *Microfluid. Nanofluid.*, **9** (2010) 1151.
- [19] McDONALD J. C., DUFFY D. C., ANDERSON J. R., CHIU D. T., WU H., SCHUELLER O. J. A. and WHITESIDES G. M., *Electrophoresis*, **21** (2000) 0173.
- [20] ANNA S. L., BONTOUX N. and STONE H. A., *Appl. Phys. Lett.*, **82** (2003) 364.
- [21] SAFFMAN P. G. and TAYLOR G. I., *Proc. R. Soc. London, Ser. A*, **245** (1958) 312.
- [22] HOMS Y. G. M., *Annu. Rev. Fluid Mech.*, **19** (1987) 271.